JOURNAL OF APPLIED ELECTROCHEMISTRY **29**: 137–145, 1999.

The anode effect as a fluid dynamic problem

H. VOGT

Fachbereich Verfahrens und Umwelttechnik, Technische Fachhochschule Berlin, D-13353 Berlin, Germany

Received 29 October 1997; accepted in revised form 2 June 1998

The so-called anode effect, particularly important in industrial alumina electrolysis, has mostly been interpreted as the consequence of altered wettability of the electrode surface by the melt. By means of a mathematical model assuming isolated large bubbles in contact with the electrode it is shown that the anode effect is the result of the combined action of fluid dynamics and wettability. The interpretation of the incipience of the anode effect obtained by means of a previous, completely different mathematical model is confirmed. The theoretical results are compared with experimental data by various authors.

Keywords: *aluminium electrolysis*, *anode effect*, *fluid dynamics*, *gas evolution*, *wettability*

List of symbols

A electrode surface area (m^2)
A_r area pertinent to one bubble at the electrode (m^2)
b Laplace parameter, Equation 12 (m)
C_1 constant
C_2 constant ($A\,m^{-2}$)
f_G gas evolution efficiency
f_I fraction of the current passing through the electrode side walls
F Faraday constant, $F = 96\,487\,A\,s\,mol^{-1}$
F force ($kg\,m\,s^{-2}$)
g acceleration due to gravity ($m\,s^{-2}$)
h vertical coordinate (m)
H bubble height (m)
I total current (A)
j nominal current density ($A\,m^{-2}$)
L length of electrode edge crossed by bubbles (m)
L_1 side length of microarea A_r m
m exponent, Equation 19
n charge number
n_r number of bubbles
p pressure ($kg\,m^{-1}\,s^{-2}$)
R universal gas constant, $R = 8.3143\,kg\,m^2\,s^{-2}\,mol^{-1}\,K^{-1}$
R radius (m)
R_0 radius of the contact area, Fig. 2 (m)
R_s radius of the projected area, Fig. 2 (m)
t time (s)
T temperature (K, °C)
v bubble velocity ($m\,s^{-1}$)
V bubble volume (m^3)
$\dot{V}_G$ volume flow rate of gas ($m^3\,s^{-1}$)
x horizontal coordinate (m)
y coordinate perpendicular to the electrode surface (m)

Greek symbols
α angle of inclination
β angle, Equation (A9)
γ surface tension ($kg\,s^{-2}$)
ε current efficiency
η_L dynamic liquid viscosity ($kg\,m^{-1}\,s^{-1}$)
ϑ contact angle (°)
Θ fractional bubble shielding of the electrode surface
ν stoichiometric number
ρ_G gas density ($kg\,m^{-3}$)
ρ_L liquid density ($kg\,m^{-3}$)
τ shear stress ($kg\,m^{-1}\,s^{-2}$)

Subscripts
a advancing
b critical
r receding

1. Introduction

Robert Bunsen, who was the first to prepare aluminium by electrolysis [1], was also the first to observe and describe the anode effect [2]. It is striking that, although during the past almost 150 years numerous attempts were made to clarify the cause of the anode effect in aluminium electrolysis, a definite and generally accepted explanation could not be given. The phenomena of the anode effect and the available interpretations have been compiled repeatedly [3–9].

The most conclusive interpretations may be summarized according to the following three headings:

(a) *Excessive increase in the concentration* (*diffusion*) *overpotential*. It is known that the cell voltage increases when the bulk concentration of reactant (O^{-2}) drops below a value where the interfacial concentration at a certain current density tends to zero. Since the anode effect in alumina reduction cells always occurs at low Al_2O_3 concentrations and can be overcome by addition of

fresh Al_2O_3, that interpretation is obvious [4]. Nonetheless, there are difficulties in explaining the phenomenon of a very rapid increase in the cell voltage of industrial cells [10] characteristic of the incipience of the anode effect simply by the gradual dilution of alumina.

(b) *An electrically insulating layer of a solid phase forms on the anode*. The oldest attempt to interpret the onset of the anode effect was made by Bunsen who supposed an electrically insulating layer of silicon or lime [3]. This explanation turned out to be unsuitable for Al_2O_3 electrolysis, but other workers clung to the idea of an insulating layer of solid material and believed in AlF_3 or solid graphite fluoride [7, 11]. Those explanations fail because the anode effect has also been observed at inert electrodes [12, 13]. For carbon anodes, the process of solid formation would be too slow or the products thermally unstable [7].

(c) *A layer of a gaseous phase forms blanketing the anode*. Two fundamentally different reasons have been considered. One of these attributes the effect to an change in wettability of the anode. Such a change may occur for various reasons. Arndt and Probst [14] observed that the volume of gas bubbles underneath the anode depends on the Al_2O_3 concentration, and they argued for variable wettability. The finding was confirmed by numerous investigations and was explained by the action of surface active species such as Al^{3+}, Na^+ or the cryolite ratio [5, 15]. Another view was proposed by Wartenberg [16]. Based on the previous findings of Coehn and Neumann [17] obtained in aqueous solutions, he concluded that the impact of the electrical charge of the gas–liquid interface on wetting may be the cause of the anode effect. It is further known that electrocapillarity affects the solid–liquid interfacial tension, hence, the wettability expressed by the contact angle [15] as already shown by Möller in 1909 [18]. Furthermore, it has been found that the wettability is affected by the kind of anode material, particularly its porosity [19], the effect of which may be superimposed on that of the electrocapillarity. When Arndt and Probst, nearly 75 years ago, investigated anodes of various porosity they found that "large porosity is inimical to the anode effect" [14]. The finding has been confirmed by recent investigations. The wettability may further be affected by the adsorption of gases at the anode surface, such as F_2 or CF_4 [6, 7] which may form at low values of Al_2O_3 concentration.

A completely different view was established by Mazza and coworkers [20] who used 'Helmholtz instability' instead of wettability to explain the onset of the anode effect. The same workers later confined the effect of the instability to the region of large Al_2O_3 concentrations [21]. Furthermore, since the mechanism of bubble detachment from vertical electrodes differs substantially from that from electrode surfaces facing downwards, the action of the Helmholtz instability on the anode effect, at least in alumina reduction cells, appears dubious.

Change in wettability, for whatever reason, remains as a possible and almost generally accepted cause of the anode effect. However, wettability is not a sufficient explanation. Imagine an electrode constructed with a completely surrounding wall to prevent the evolved gas from being released. Initially the electrode surface is completely in contact with the electrolyte. After some time from the start, the electrode will be completely covered with bubbles. The anode effect must necessarily occur, irrespective of the wettability. One must conclude that the anode effect cannot be explained on a static basis. It appears reasonable to establish a concept that takes into account the following aspects: (i) That the balance of the rate of production of gas and the rate of removal of gas, at steady state, are equal, and (ii) that, as is known from early experimental investigations [22], during the occurrence of the anode effect, the anode is blanketed by a continuous (or quasi-continuous) gas film. This finding suggests that the condition for the incipience of the anode effect is met if the distance between the gas bubbles in contact with the electrode surface is diminished to such an extent that the bubbles begin blanketing the electrode surface. The resulting large increase in ohmic resistance and overpotential is accompanied by a large decrease in current and/or increase in cell voltage.

A convincing interpretation of the onset of the anode effect may be expected, if both aspects can be put into a causal and quantitative interrelation. The wettability is assumed to play an important role.

The same basic ideas have served to establish a model based on the assumption of a layer containing a dispersion of finely dispersed small bubbles underneath the electrode [23]. The conformity of the model with reality has been considered questionable. It is the object of the present paper to establish an alternative model assuming single large bubbles moving in contact with the electrode.

2. Gas rates

2.1. *Rate of gas evolution*

The rate of gas evolved at the anode is given by Faraday's law:

$$\frac{\dot{V}_G}{A} = \frac{jRT\varepsilon}{(n/v)Fp} f_G(1 - f_I) \tag{1}$$

$$\text{where} \quad j \equiv I/A \tag{2}$$

denotes the nominal current density, and f_G denotes the gas evolution efficiency (i.e., the fraction of the total amount of electrochemically generated substance(CO_2/CO evolved as gas in form of bubbles grown at the electrode surface [24]). Equation 1 takes

account of the fact that the vertical side walls of the electrodes are exposed to the electrolyte and absorb a fraction f_I of the total current I [25].

2.2. *Rate of gas removal*

Large gas bubbles underneath the anode move in contact with the anode surface and leave the underside of the electrode passing across the electrode edge of length L. This length may be the total perimeter of the electrode (as probably correct for the monolithic Söderberg anodes) or only a part of the perimeter (as in cells with a multitude of prebaked anodes separated by open gaps). On the way from the active nucleation site to the edge, the bubbles grow to a final volume V by desorption of dissolved gas evolved and, possibly additionally, by coalescence [26] and by engulfing smaller bubbles adhering to the electrode (scavenger effect). If a number n_r of bubbles leaves the electrode across the length L during the time t, the total gas flow rate is

$$\dot{V}_G = \frac{n_r V}{t} \tag{3}$$

Consider a gas bubble of average shape and size at the edge immediately before leaving the underside with an average velocity v. At that position, a certain microarea

$$A_r = L_1 \frac{L}{n_r} \tag{4}$$

may be attributed each bubble, Fig. 1. The residence time of a bubble in contact with that area is

$$t = \frac{L_1}{v} \tag{5}$$

Each bubble with a contact angle $\vartheta \geq 90°$ covers a partial area πR_s^2 of the microarea A_r, where R_s denotes the radius of the contacting area $R_s = R_0$, Fig. 2. Bubbles with a contact angle $\vartheta \leq 90°$ shadow the area πR_s^2, where R_s is the maximum mean bubble radius. Introducing a fractional bubble shielding of the electrode surface [27] applicable to bubbles of arbitrary values of the contact angle

$$\Theta \equiv \frac{\pi R_s^2}{A_r} \tag{6}$$

and combining Equations 3–6 gives

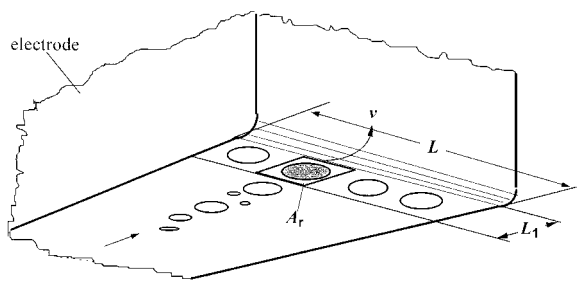

Fig. 1. Flow of gas bubbles along the underside of the electrode surface.

$$\frac{\dot{V}_G}{A} = \frac{VLv\Theta}{A\pi R_s^2} \tag{7}$$

2.3. *Mass balance*

Combination Equations 1 and 7 gives, for steady state operation,

$$\frac{j\varepsilon f_G(1-f_I)\,RT}{(n/v)F\,p\,v\Theta}\,\frac{\pi\,R_s^2 A}{VL} = 1 \tag{8}$$

3. Bubble volume

The shape of gas bubbles adhering to an electrode surface facing upwards may be described with sufficient accuracy by that of a truncated sphere [28]. This is not generally admissible for large bubbles in aluminium electrolysis for two reasons. First, large bubbles are flattened, and their height cannot exceed a maximum value to be calculated separately from the balance of forces. Secondly, bubbles moving underneath and in contact with a solid phase exhibit varying contact angles. At the front of the moving bubble, the contact angle (advancing angle) is smaller than at the rear (receding angle).

With respect to the difficulties and uncertainties in the estimation of the real shape of large bubbles a first approximation will be used. It will be shown that it is satisfactory to substitute the real bubble shape by that of a vertical cylinder of height H and radius R_s, Fig. 2. For values of the contact angle $\vartheta \leq 90°$, the radius R_s coincides with the radius of the circle obtained by orthogonal projection. For values $\vartheta \geq 90°$, the maximum projected radius coincides with the radius of the contact area, $R_0 = R_s$. The bubble volume is

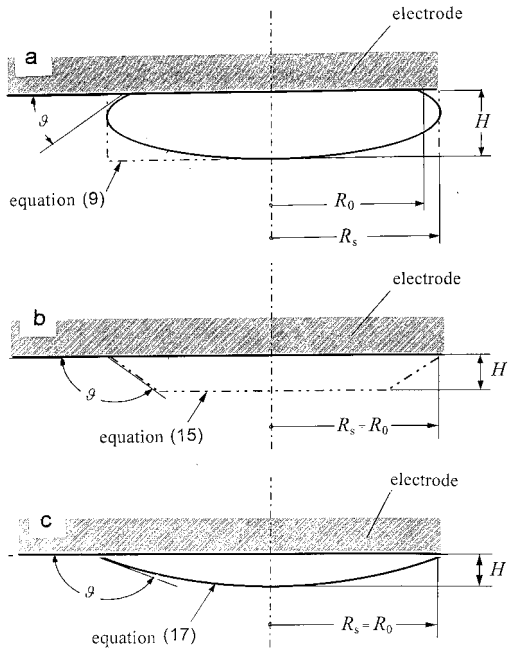

Fig. 2. Bubble geometry and approximations (a) Equation 9 for $\vartheta \leq 90°$; (b) Equation 15 for $90° \leq \vartheta \ll 180°$; (c) Equation 17 for $\vartheta \to 180°$.

$$V = \pi R_s^2 H \tag{9}$$

Inserting Equation 9 into Equation 8 gives

$$\frac{j\varepsilon f_G(1-f_I)RT}{(n/v)F\,p\,v\Theta}\frac{A}{HL} = 1 \tag{10}$$

The value of the bubble height H can be estimated. For large gas bubbles underneath a horizontal plane, the height agrees approximately with the above mentioned maximum height estimated from a balance of forces in Appendix 1:

$$H = \left[\frac{2\gamma}{(\rho_L - \rho_G)g}(1+\cos\vartheta)\right]^{1/2} = b(1+\cos\vartheta)^{1/2} \tag{11}$$

where

$$b \equiv \left[\frac{2\gamma}{(\rho_L - \rho_G)g}\right]^{1/2} \tag{12}$$

is the Laplace parameter.

4. Critical condition

As pointed out above, the cell operation approaches a critical state if the velocity v of bubble removal is too low to remove separate bubbles. The critical current density, $j = j_c$, characterizing the onset of the anode effect is reached when the fractional surface coverage Θ attains large values near unity. Then a large fraction of the total electrode area is covered with gas bubbles, the cross-sectional area for transport of CO_2/CO in dissolved form from the electrode is substantially lowered. A large fraction f_G of the dissolved gas generated is transformed into the gaseous phase of the bubbles [24]. The value of f_G and Θ are nearly equal, $f_G/\Theta \approx 1$. Equation 10 reduces to

$$\left[\frac{j\varepsilon(1-f_I)RT}{(n/v)F\,p\,v}\frac{A}{HL}\right]_c = 1 \tag{13}$$

With equation (11) the critical current density takes the form

$$j_c = \frac{(n/v)F\,p\,v}{\varepsilon(1-f_I)RT}\frac{bL}{A}(1+\cos\vartheta)^{1/2} \tag{14}$$

5. Discussion

5.1. *Parameters*

Equation 14 represents the general experience that the critical current density is a quantity characteristic of the incipience of the anode effect. But it is seen that the critical current density depends on numerous parameters:

- wettability of the electrode, expressed by the contact angle ϑ
- composition of the gaseous phase, expressed by n/v
- current efficiency ε of the generation of dissolved gases
- conditions of state, expressed by temperature T and pressure p
- electrode size and geometry, expressed by the ratio A/L
- bubble height H, controlled by the contact angle ϑ and the properties in the Laplace parameter b, Equation 12
- bubble size, expressed by R_s
- velocity of bubble removal v, affected in particular by the inclination and shape of the electrode surface and the geometry of the interelectrode space, but also by the viscosity of the melt.

Some of these parameters are mutually interrelated. The contact angle controls the shape of the bubble and the height H. The temperature acts on the volume gas rate of the gas evolution and on the viscosity of the melt, hence on the velocity v. The contact angle affects the current density, but the latter is affected by the current density, because of electrocapillarity as confirmed in experiment [15].

5.2. *Fractional bubble shielding*

According to the applied model, the incipience of the anode effect is linked with the condition $\Theta \to 1$ merely *at the edge* of the anode. That is a sufficient condition. Supposing that the edge of the electrode is completely covered with gas bubbles and the rest of the electrode is free, then this implies that the local current density on the wetted area increases, activating nucleation sites and initiating growth of new bubbles which soon blanket the whole electrode surface. This process was also observed on the laboratory scale [29].

5.3. *Electrode size*

The ratio A/L in Equation 14 (approximately equal to $0.23\,A^{1/2}$ in Söderberg cells) generally increases with electrode area A showing the effect of the electrode size on the critical current density. Observations confirm that the critical current density is lower at large cells than at small cells (at a given alumina concentration). At a constant current density of $7500\,A\,m^{-2}$ the initiation of the anode effect in a laboratory cell was observed with an alumina content of 0.2–0.4%, in an industrial cell with 1–2% [10]. It is remarkable that the effect of the electrode area A already contained in Piontelli's 1965 empirical formula for the critical current density [6], although considered dubious [7], turns out to be justified.

5.4. *Bubble flow and electrode shape*

The effect of the flow on the incipience of the anode effect is supported by several experimental findings. Drossbach [30] found an essential increase in the critical current density when a horizontal electrode facing downwards was turned to a vertical position. Since the effect cannot be attributed to an increase in

the wettability, he explained the phenomenon in assuming that the pores of an anode facing downwards are filled with gas and the current is only transported across protruding peaks, whereas the gas can escape from the pores as soon as the anode is turned upwards [30]. Equation 14 explains the effect simply by the fact that an alteration in the position of the electrode surface substantially affects the flow conditions and the velocity of removal of contacting bubbles.

The finding has been confirmed repeatedly [31, 32] and is in agreement with the fact that the critical current density strongly depends on the shape of the anode as investigated by Piontelli *et al.* [6, 33, 34]. This also agrees with the finding that if the electrode surface is inclined, the bubble is subject to a stronger buoyancy force, resulting in an increased velocity as known from natural convective heat transfer at inclined plates [35] and from the flow of laminar and turbulent liquid films on surfaces inclined by an angle α according to $v \sim \sin\alpha$ and $v \sim (\sin\alpha)^{5/8}$, respectively. Experimental investigations by Ngoya [36] show that the ohmic resistance of a layer of bubbles underneath an electrode strongly decreases if the electrode is inclined by only a few degrees, thus reflecting the effect of velocity.

It is further remarkable that the experiments of Thonstad [37], carried out with forced flow, gave values of the critical current density which were much larger than in other experiments carried out with quiescent melt. Sufficiently large forced flow is able to quickly remove gas bubbles, and hence increases the critical current density (Equation 14).

5.5. *Vibrated electrodes*

Piontelli and coworkers [6, 33] found that mechanical vibration of electrodes increased the critical current density. The effect was greater for horizontal surfaces facing downwards than for cylindrical ones. This observation also harmonizes with the outcome of the model. Additional mechanical forces acting on the bubbles enhance their movement, and the action is the more effective the smaller the buoyancy flow.

5.6. *Fast voltage increase*

Although the anode potential is not a parameter contained in Equation 14, the model result is able to explain the excessive and very rapid increase in the cell voltage immediately prior to the onset of the anode effect as observed with industrial cells [10]. As the fractional bubble shielding Θ approaches unity, the local current density on the remaining wetted electrode area (in constant nominal current density) attains large values resulting in correspondingly large values of the ohmic potential drop and the anodic overpotential.

5.7. *Anodes and cathodes*

There are no parameters in Equations 14 which would suggest a restriction to anodes. Indeed, the anode effect has been observed for both anodes and cathodes [34].

5.8. *Approximated bubble volume*

For large values of contact angle, the approximation of the bubble volume by the shape of a cylinder, Equation 9, results in too large values of bubble volume. Another approximation, more appropriate for values of contact $\vartheta > 90°$ (although not for $\vartheta \to 180°$) would be that of a disc of thickness H cut from a sphere, Fig. 2(b),

$$V = \frac{\pi R_s^2 H}{2}\left\{1 + \frac{1}{3}\left(\frac{H}{R_s}\right)^2 - \left[\frac{H}{R_s} + \tan(\vartheta - 90°)\right]^2 + (\sin\vartheta)^{-2}\right\} \quad (15)$$

Combination with Equation 11 gives

$$j_c = \frac{(n/v)F\,p\,v}{RT\varepsilon}\frac{H}{2L}\left\{1 + \frac{1}{3}\left(\frac{H}{R_s}\right)^2 - \left[\frac{H}{R_s} + \tan(\vartheta - 90°)\right]^2 + (\sin\vartheta)^{-2}\right\} \quad (16)$$

In the region $\vartheta \to 180°$ Equation 15 gives values which are too small. A reasonable approximation is that of a truncated sphere, Fig. 2(c):

$$V = \frac{\pi R_s^2 H}{2}\left[1 + \frac{1}{3}\left(\frac{H}{R_s}\right)^2\right] \quad (17)$$

The approximated bubble volumes after inserting Equation 11 into Equations 9, 15 and 17 are shown in Fig. 3. The various approximated bubble volumes exhibit substantial differences, but a numerical analysis shows that their impact on the critical current density is negligibly small. Therefore, the approximation of the bubble shape by a cylinder is fully satisfactory. Equation 14 applies to all values of contact angle.

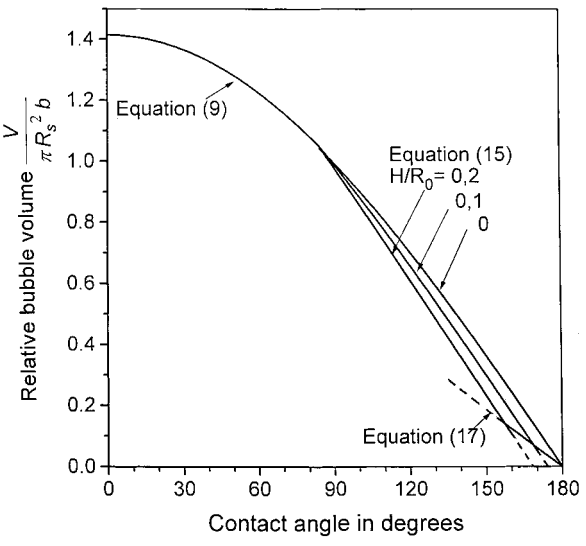

Fig. 3. Approximated bubble volumes.

6. Bubble velocity

A final consideration may be devoted to the velocity v of bubbles past the electrode surface. Experience shows that the velocity of bubbles gliding along underneath an inclined surface (as well as that of liquid drops on a solid surface) increases with the height of the bubbles (or the drops). The bubble velocity in Equation 14 decreases as the contact angle increases. The effect of the bubble height on the velocity is estimated in Appendix 2.

The edge of anodes in alumina reduction cells are rounded off [25], and the movement of the bubbles is induced or favoured by the inclination of that zone and is hampered by the wetting force. Any additional shear force at the gas–liquid interface may favour or hamper the bubble velocity depending upon its direction. A balance of these forces results in the bubble velocity underneath the electrode

$$v = \frac{(\rho_L - \rho_G) g \sin\alpha}{3\eta_G} H^2 \left\{ 1 - \frac{1.5}{H(\rho_L - \rho_G) g \sin\alpha} \times \left[\frac{4\gamma R_0 \Delta\vartheta \sin\vartheta}{\pi R^2} - \tau_{y=H} \right] \right\} \quad (18)$$

It is seen that the velocity increases as the bubble height increases. The relationship may be approximated by

$$v = C_1 H^m \quad (19)$$

where the exponent $m > 1$ is generally smaller or larger than 2. Neglecting the shear force $\tau_{y=H}$ results in $m > 2$; additionally neglecting the wetting force gives $m = 2$. The critical current density results, after combination of Equations 19 and 14 and considerating Equation (11), in

$$j_c = C_1 \frac{(n/v) F p L H^{1+m}}{\varepsilon(1 - f_I) RTA} = C_1 \frac{(n/v) F p L b^{1+m}}{\varepsilon(1 - f_I) RTA} (1 + \cos\vartheta)^{(1+m)/2} \quad (20)$$

For a given system, the effect of the contact angle may be expressed by

$$j_c = C_2 (1 + \cos\vartheta)^{(1+m)/2} \quad (21)$$

where C_1 and C_2 are empirical constants. Equation 21 is shown in Fig. 4 for a value $m = 2$ and two selected values C_2. The graph exhibits the form similar to a reverse S-shaped curve as already previously found by means of a fundamentally different model [23].

The effect of the contact angle on the critical current density was experimentally studied by Karpachev and coworkers [38] and by Beljaev and coworkers [39] some decades ago and more recently by Qiu and coworkers [40]. Their results are shown in Fig. 4 and correlated by various values of C_2 reflecting different operating conditions. The agreement with the theoretical Equation 21 is satisfactory in the light of the substantial experimental difficulties.

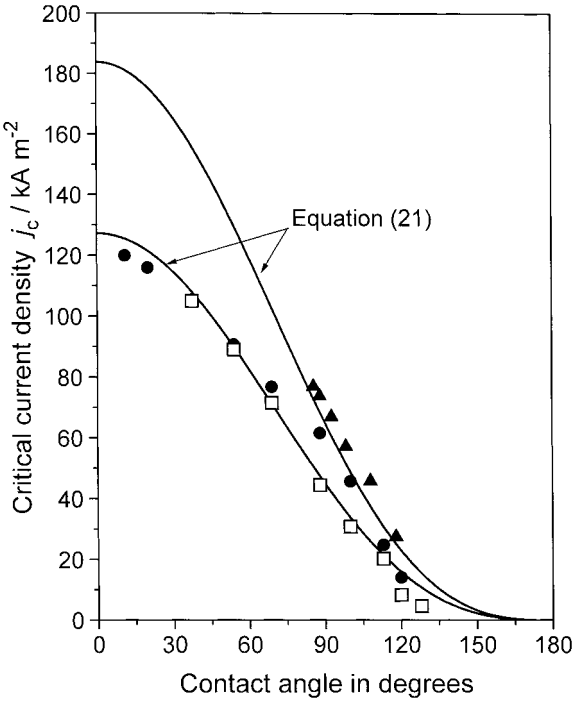

Fig. 4. Comparison of Equation 21 with experimental data in the system $Na_3AlF_6 - Al_2O_3$ at $T = 1000\,^\circ C$. Key: (□) Karpachev *et al.* [38] and (●) Beljaev and Kusmin [39] with $C_2 = 45\,A\,m^{-2}$, $m = 2$; (▲) Qiu *et al.* [40] with $C_2 = 65\,A\,m^{-2}$, $m = 2$.

Papers [38–40] relate the contact angle and the critical current density separately to the alumina content. Although the measured values of the first two papers diverge strongly from [40] Fig. 4 shows not more than moderate deviations from each other.

The previous model based on the assumption of a bubble layer containing dispersed small bubbles has been shown to be appropriate for correlating the experimental data [23]. The agreement of the result of the present model assuming single large bubbles in contact with the electrode with the same experimental data shows that the particular configuration of the gas–liquid dispersion is not very influential on the critical current density. Each of the models demonstrates equally well that the anode effect is the result of a combined action of wettability and fluid dynamics. This result is of relevance for industrial molten salt electrolysis where both types of gas–liquid configuration occur [8]. Observations by Drossbach and Krahl [41] might also lead to the conclusion that, at least under certain conditions, a mixed configuration of large bubbles and much smaller ones may be encountered.

7. Historical note

From numerous observations with various electrode forms and from the different behaviour of vibrated and motionless electrodes, Piontelli, Mazza and Pedeferri have recognized that wettability alone is not sufficient to explain the anode effect. In the mid-1960s they wrote: "The wetting properties of the anode surface are obviously important. On the other hand, the dynamic aspects of the anode effect ... could

hardly be realized by considering merely changes in time of the wetting properties. [33].'' As a consequence, Mazza and coworkers [20, 32] proposed the Helmholtz instability, which had been found useful in the analogous event in boiling. For aluminium electrolysis, that interpretation cannot satisfy for the above reasons and has already been restricted or withdrawn by the authors themselves [21].

A further interesting remark can be found in a paper of 1987 by Qiu and Zhang [13]. To overcome contradictions in a previous interpretation of the incipience of the anode effect, a second type was proposed as occurring by accumulation of gas, if the rate of gas evolution on the anode exceeds the rate of gas release*. That interpretation may hold for extraordinary conditions, possibly for the initial anode effect, but fails for steady-state operation where the mass balance, Equation 8, continues to be valid irrespective of any changes in the wettability. Nonetheless, the authors clearly recognized that the anode effect is initiated by a 'hydrodynamic process' [13].

8. Conclusion

The condition for the incipience of the anode affect is met, if the velocity of gas bubbles gliding along underneath the anode surface drops below a critical value v_c, characterized by the condition that the distance between neighbouring bubbles diminishes to such an extent that the bubbles contact each other tending to form a continuous gas film. The cross-sectional area for transport of charge and of reactant and product is substantially reduced; the cell voltage increases and/or the current density drops very fast.

That critical bubble velocity depends on numerous parameters. It is affected by the size and shape of the electrode surface and its inclination, and further by the flow velocity of the melt which, in turn, is controlled by the geometry of the interelectrode space and the operating conditions, notably temperature. Increased temperature lowers the viscosity.

Of course, the critical bubble velocity is affected by the volume rate of gas evolution. Therefore, it is reasonable to speak of a critical current density which, however, is not a sufficient parameter. It depends on the composition of the anode gas (CO_2 and CO) as well as on temperature and pressure and, moreover, on the current efficiency of the generation of dissolved gas.

An important role must be attributed to the wettability of the electrode directly controlling the shape of the gas bubbles underneath the electrode. The model result agrees with experimental findings.

The particular configuration of gas–liquid dispersions in industrial processes appears to have no essential impact on the critical current density.

*Strictly, the opposite process occurs: A deterioration of the wettability, i.e. an increase in the contact angle, decreases the bubble volume and lowers the gas hold-up in the cell. The incipience of the anode effect (under constant current condition) is accompanied by a continuous diminution of the gas cumulation.

Appendix 1: The height of large bubbles

The static pressure gradients in the gaseous phase and in the liquid phase are

$$\frac{dp_G}{dh} = -\rho_G g \tag{A1}$$

$$\frac{dp_L}{dh} = -\rho_L g \tag{A2}$$

Substraction

$$d(p_G - p_L) = (\rho_L - \rho_G) g dh \tag{A3}$$

and integration gives

$$(p_G - p_L) - (p_G - p_L)_{h=0} = (\rho_L - \rho_G) gh \tag{A4}$$

On the other hand, the overpressure in the gas bubble is interrelated with the curvature of the interface according to

$$p_G - p_L = \gamma\left(\frac{1}{R_1} + \frac{1}{R_2}\right) \tag{A5}$$

where R_1 and R_2 are the main radii of curvature, Fig. 5, to result in

$$\gamma\left(\frac{1}{R_1} + \frac{1}{R_2}\right) - \gamma\left(\frac{1}{R_1} + \frac{1}{R_2}\right)_{h=0} = (\rho_L - \rho_G) gh \tag{A6}$$

Neglecting the difference between advancing angle and receding angle of moving bubbles and assuming a rotationally symmetrical form, that is, $R_1 = R_2$ at $h = 0$, gives

$$\left(\frac{1}{R_1} + \frac{1}{R_2}\right) - \frac{2}{R_{h=0}} = \frac{(\rho_L - \rho_G) gh}{\gamma} \tag{A7}$$

For the sake of simplicity, two simplifications will be introduced applicable to large bubbles:

$$R_{h=0} \to \infty$$

$$R_2 \gg R_1, \text{unless } R \to \infty$$

where R_1 is the radius in the plane of the Figure. The laws of geometry give

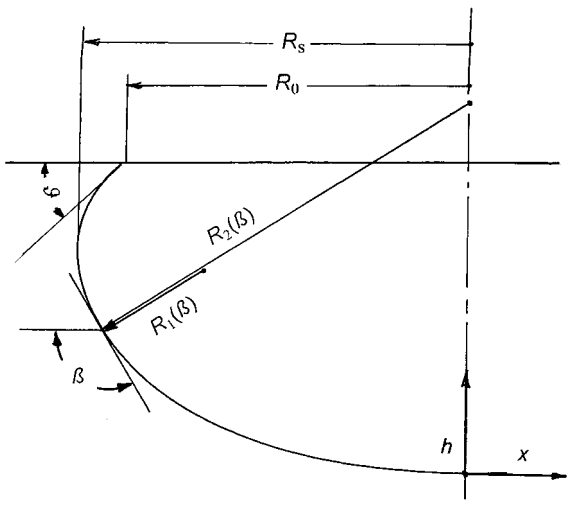

Fig. 5. Geometry of a bubble underneath a horizontal surface.

$$\frac{1}{R_1} = \frac{d^2x/dh^2}{[1 + (dx/dh)^2]^{1.5}} \quad \text{(A8)}$$

with

$$\frac{dx}{dh} = -\tan[\beta(h) - 90^\circ] \quad \text{(A9)}$$

Combination of Equations A7 and A8 and integration with the boundary condition $\beta = \theta$ at $h = H$ gives the simplified contour of the bubble:

$$\frac{(\rho_L - \rho_G)g}{\gamma}\left(\frac{H^2 - h^2}{2}\right) = \left(\frac{H}{b}\right)^2\left[1 - \left(\frac{h}{H}\right)^2\right] = \cos\vartheta - \cos\beta \quad \text{(A10)}$$

Particularly at $h = 0$ the angle is $\beta = 180^\circ$, directly resulting in Equation 11.

Appendix 2: Bubble velocity

Several forces act on a gas bubble gliding underneath an electrode.

(i) The difference in *buoyancy force* and *gravitational force* at the inclined zone of the electrode surface near the edge

$$F_1 = V(\rho_L - \rho_G)g\sin\alpha = y\pi R^2(\rho_L - \rho_G)g\sin\alpha \quad \text{(A11)}$$

where α denotes the angle of inclination, y is the coordinate perpendicular to the surface.

(ii) The *wetting force*

$$F_2 = \pi\gamma R_0\left[\cos\left(\vartheta - \frac{2}{\pi}\Delta\vartheta_a\right) - \cos\left(\vartheta + \frac{2}{\pi}\Delta\vartheta_r\right)\right] \approx 4\gamma R_0\Delta\vartheta\sin\vartheta \quad \text{(A12)}$$

where ϑ represents the contact angle of the bubble not distorted by the acting forces. $\vartheta - \Delta\vartheta_a$ is the advancing angle, $\vartheta + \Delta\vartheta_r$ the receding angle, applicable to the range $\Delta\vartheta_a \le \vartheta \le 180^\circ - \Delta\vartheta_r$, $\Delta\vartheta_r \approx \Delta\vartheta_a = \Delta\vartheta$.

(iii) The *shear force, F_3, in laminar flow inside* the flat bubble

$$F_3 = \pi R^2\tau = -\pi R^2\eta_G\frac{dv}{dy} \quad \text{(A13)}$$

(iv) Generally, an additional *shear force, F_4, at the gas–liquid interface* of the bubble, $y = H$,

$$F_4 = \tau_{y=H}\pi R_s^2 \quad \text{(A14)}$$

From the balance of forces,

$$F_2 + F_4 - F_1 - F_3 = 0 \quad \text{(A15)}$$

follows the velocity profile

$$v(y) = \frac{(\rho_L - \rho_G)g\,\sin\alpha}{\eta_G}\left(Hy - \frac{y^2}{2}\right) - \frac{4\gamma R_0\Delta\vartheta\,\sin\vartheta}{\pi R^2\eta_G}y + \frac{\tau_{y=H}}{\eta_G}y \quad \text{(A16)}$$

after integration with the two boundary conditions

$$v = 0 \quad \text{at} \quad y = 0$$

and

$$\frac{dv}{dy} = -\frac{4\gamma R_0\Delta\vartheta\sin\vartheta}{\pi R^2\eta_G} + \frac{\tau_{y=H}}{\eta_G} \quad \text{at} \quad y = H$$

Integration over the bubble height

$$v \equiv \int_0^H v\frac{dy}{H} \quad \text{(A17)}$$

yields the desired bubble velocity, Equation 18.

References

[1] Anon. [F. Wöhler ?], *Ann. Chemie Pharm.* **92** (1854) 252.
[2] R. Bunsen, [*Poggendorff's*] *Ann. Physik* **92** (1851) 648.
[3] G.-E. Taylor, *Trans. Am. Electrochem. Soc.* **47** (1925) 301.
[4] L. Ferrand, 'Histoire de la science et des techniques de l'aluminium et ses developements industriels', Vol. 1 (Humbert, Largentière, 1960).
[5] A. I. Beljaev, *in* A. I. Beljaev (Ed.), 'Surface Phenomena in Metallurgical Processes' (Consultants Bureau, New York 1965), p. 3.
[6] R. Piontelli, B. Mazza and P. Pedeferri, *Metall. ital.* **57**(2) (1965) 1.
[7] K. Grjotheim, C. Krohn, M. Malinovský and J. Thonstad, 'Aluminium Electrolysis' (Aluminium-Verlag, Düsseldorf, 1982).
[8] U. Erikson and R. Tunold, Proceedings of the International Sympsium on Molten Salts (edited by G. Mamantov) The Electrochemical Society., Pennington, NJ (1987); 87–7, p. 602.
[9] Qiu Z., *Chin. J. Met. Sci.* **8** (1992) 15.
[10] J. Thonstad, F. Nordmo, A. H. Husøy, K. ∅. Vee and D. C. Austrheim, 'Light Metals **1984**' (edited by J. P. McGeer) Warrendale (1984), p. 825.
[11] D. Devilliers, F. Lantelme and M. Chemla, *Electrochim. Acta* **31** (1986) 1235.
[12] E. W. Dewing and E.T. van der Kouwe, *J. Electrochem. Soc.* **124** (1977) 58.
[13] Qiu Z. and Zhang M., *Electrochim. Acta* **32** (1987) 607.
[14] K. Arndt and H. Probst, *Z. Elektrochemie* **29** (1923) 323.
[15] Qiu Z., Wei Q. and You K., 7th Int. Leichtmetalltagung, Leoben-Wien (1981), p. 256.
[16] H. von Wartenberg, *Z. Elektrochemie* **32** (1926) 330.
[17] A. Coehn and H. Neumann, *Z. Physik* **23** (1923) 54.
[18] H. G. Möller, *Z. Phys. Chemie* **65** (1909) 226.
[19] A. I. Beljaev, E. A. Zhemchuzhina and L. A. Firsanova, Physikalische Chemie geschmolzener Salze. Dt. Verlag für Grundstoffindustrie, Leipzig (1964).
[20] B. Mazza, P. Pedeferri, R. Piontelli and A. Tognoni, *Electrochim. Metall.* **2** (1967) 385.
[21] B. Mazza, P. Pedeferri and G. Re, *Electrochim. Acta* **23** (1978) 87.
[22] W. Muthmann, H. Hofer and L. Weiss, *Ann. Chemie* **320** (1902) 231.
[23] H. Vogt, *Electrochim. Acta* **42** (1997) 2695.
[24] *Idem*, *ibid.* **29** (1984) 167.
[25] J. Zoric, I. Roušar and J. Thonstad, *J. Appl. Electrochem.* **27** (1997) 916.
[26] T. Utigard and J. M. Toguri, 'Light Metals **1986**' (edited by R. E. Miller), Warrendale (1986), p. 405.
[27] H. Vogt, *Electrochim. Acta* **25** (1980) 527.
[28] P. L. King and B. J. Welch, *J. Appl. Electrochem.* **2** (1971) 23.
[29] P. Drossbach, T. Hashino, P. Krahl and W. Pfeiffer, *Chemie-Ing.-Technik* **33** (1961) 84.
[30] P. Drossbach, *Z. Elektrochem.* **55** (1951) 38.
[31] N. Watanabe, Y. Fujii and S. Yoshizawa, *J. Electrochem. Soc. Japan* **31** (1963) 131.
[32] B. Mazza, P. Pedeferri and A. Tognoni, *Chimica Ind.* **53** (1971) 123.

[33] R. Piontelli, B. Mazza and P. Pedeferri, *Electrochim. Acta* **16** (1965) 1117.
[34] R. Piontelli, B. Mazza, P. Pedeferri and A. Tognoni, *Electrochim. Metall.* **2** (1967) 257.
[35] T. Fujii and H. Imura, *Int. J. Heat Mass Transfer* **15** (1972) 755.
[36] F. N. Ngoya, 'The Effect of Electrolytic Gas Evolution on Conductivity'. Dissertation of the University of Dar es Salaam (1983).
[37] J. Thonstad, *Electrochim. Acta* **12** (1967) 1219.
[38] W. Karpachev, I. L. Dolgov and N. M. Kanchinski, *Legkie Metally* **3**(2), (1934), 20; *Chem. Zentralbl.* **105** (1934) 3830.
[39] A. I. Beljaev, M. B. Rapoport and L. A. Firsanova, 'Metallurgie des Aluminiums', Vol. 1 (Verlag der Technik, Berlin 1956), p. 121.
[40] Qiu Z., Wei C. and Chang M., 'Light Metals 1982' edited by J. E. Andersen (Metallurgical Soc. AIME, Warrendale 1982), p. 279.
[41] P. Drossbach and P. Krahl, *Z. Elektrochemie, Ber. Bunsenges* **62** (1958) 178.